A deployable, annular, 30m telescope, space-based observatory

Justin J. Rey*[a], Allan Wirth[a], Andrew Jankevics[a], Franklin Landers[a], David Rohweller[b], C. Bill Chen[c], Allen Bronowicki[c]. [a]Northrop Grumman AOA-Xinetics, 115 Jackson Rd, Devens, MA, USA 01434; [b]Northrop Grumman Astro Aerospace, 6384 Via Real, Carpinteria, CA, USA 93013-2920, [c]Northrop Grumman Aerospace Systems, One Space Park, Redondo Beach, CA, USA 90278

ABSTRACT

High resolution imaging from space requires very large apertures, such as NASA's current mission the James Webb Space Telescope (JWST) which uses a deployable 6.5m segmented primary. Future missions requiring even larger apertures (>>10m) will present a great challenge relative to the size, weight and power constraints of launch vehicles as well as the cost and schedule required to fabricate the full aperture. Alternatively, a highly obscured annular primary can be considered. For example, a 94% obscured 30m aperture having the same total mirror area ($78m^2$) as a 10m unobscured telescope, can achieve 3X higher limiting resolution performance. Substantial cost and schedule savings can be realized with this approach compared to fully filled apertures with equivalent limiting resolution. A conceptual design for a ring-shaped 30m telescope is presented and the engineering challenges of its various subsystems analyzed. The optical design consists of a 20X annular Mersenne form beam compactor feeding a classical 1.5m TMA telescope. Ray trace analysis indicates the design can achieve near diffraction limited images over a 200μrad FOV. The primary mirror consists of 70 identical rectangular 1.34x1.0m segments with a prescription well within the demonstrated capabilities of the replicated nanolaminate on SiC substrate technology developed by AOA Xinetics. A concept is presented for the deployable structure that supports the primary mirror segments. A wavefront control architecture consisting of an optical metrology subsystem for coarse alignment and an image based fine alignment and phasing subsystem is presented. The metrology subsystem is image based, using the background starfields for distortion and pointing calibration and fiducials on the segments for measurement. The fine wavefront control employs a hill climbing algorithm operating on images from the science camera. The final key technology required is the image restoration algorithm that will compensate for the highly obscured aperture. The results of numerical simulations of this algorithm will be presented and the signal-to-noise requirements for its successful application discussed. It is shown that the fabrication of the 30m telescope and all its supporting subsystems are within the scope of currently demonstrated technologies. It is also shown that the observatory can be brought to geosynchronous orbit, in its entirety, with a standard launch vehicle.

Keywords: ring telescope, thinned, sparse aperture, compact, segmented, replicated optics, silicon carbide, AstroMesh

1. INTRODUCTION

As the capability of space-based observatories has grown and their data products shared, whole new fields of science and industry have emerged around interpreting, organizing and extending the information they generate to greater and more prolific purposes. This is occurring in the astronomical community with releases like the Kepler exoplanet data set as well as in the geospatial intelligence (GEOINT) community with social networks like Tomnod where crowdsourcing is used to enhance satellite imagery from commercial space image vendors.

The next generation of image products from these industries will inevitably require information to be provided at greater resolution than current space-based observatories can offer. Real-time geospatial imagery is a perfect example of the paradigm. Providing a continuous stream of optical data requires an imaging asset to be located above the region of interest at all times. Geo-political factors limit the applicability of using UAV's for this concept of operations, and low-earth orbiting satellites have long gaps in coverage between transits over the region. Considering the costs to mitigate either of these approaches, real-time observation from a geosynchronous satellite provides a compelling solution. At such a greater distance, however, the technical specifications of the telescope become even more challenging than those of NASA's James Webb Space Telescope (JWST). A description of the requirements of such a system is provided.

*justin.rey@ngc.com; phone 1-978-757-9526; northropgrumman.com/BusinessVentures/AOAXinetics

2. OVERVIEW

The intent of this study is to describe both the feasibility and the technical advantages of a highly obscured, annular telescope as well as to present a context for its use. In order to properly evaluate such a design, a baseline mission was chosen where the performance characteristics of an extremely high resolution observatory would be relevant. Parameters describing the selected mission are quantified below in Figure 1.

Mission Parameter	**Value**
Imaging wavelength	.450 - .750 microns
Image quality	NIIRS 6
Image update rate	2 Hz
Imaging duration	14 days, continuous
Years of operation	2025 - 2032
High-resolution ground field of view	7.2 km
Scanning mode field of view	144 km

Figure 1. Mission Parameters

Based on the mission parameters above, many program-level requirements can be directly derived. The requirement for long duration, real-time imaging is addressed by observing at geosynchronous orbit, as described previously. This requires a heavy launch vehicle such as ULA's Atlas V, for which payload requirements are publicly available[1]. The image interpretability metric known as NIIRS 6 specifies that feature resolution as fine as 0.75m must be available for detection in the visible spectrum[2]. Additionally, at an altitude of 36,000km, Rayleigh criterion suggests achieving the required ground sample distance is only possible for telescope diameters of 30m or greater. Image noise and total telescope wavefront error also need to remain below standard thresholds or image quality will degrade below the NIIRS 6 interpretability scale. More detail on this derivation is given in the analysis section.

Level 2 Requirement	**Value**
Altitude	36 x 10^6 m
Launch vehicle	Atlas V
Payload mass	6300 kg
Payload volume	4.57mØ x 15.25m
Ground sample distance	0.750 m
Primary mirror diameter	30 m
Signal-to-noise	150:1
Wavefront error	0.055 microns

Figure 2. Level 2 Requirements

The requirement for a 30m primary mirror is clearly the greatest obstacle to mission feasibility, both in terms of its cost and launch limitations. Following historical space telescope designs, a primary surface of this diameter would contain more than 20 times the mirror area of JWST. To give an approximation of the cost of such a system, scaling only the telescope portion of such programs would on its own exceed $20B, not to mention the manufacturing and payload implications. Addressing this obstacle to launch is the focus of our design.

Employing some form of sparse aperture optimization is the most straightforward way to reduce programmatic constraints. This has been a familiar design approach for radio frequency antennae, such as the VLA facility, for many years. However, implementing the technique on optical wavelength systems presents several challenges, adeptly described by the previous authors[3]. Of particular distinction are the families of circular subaperture arrays derived by Golay due to their highly compact, non-redundant autocorrelation functions[4]. The deep base of published research in this area was essential for us in extending the study to include subaperture geometries of non-circular shape.

The most appealing design was a completely circular and fully continuous ring, having an inner diameter no greater than 94% of the outer diameter. Similar to the optimized Golay arrays, a crucial design constraint is not to leave any areas unfilled that result in spatial frequencies of the modulus of the optical transfer function (within the pupil diameter) to drop below 3% of the peak. This limit was chosen to accommodate practical noise levels, which will be shown to be very important in the simulation results section later.

The fill factor achieved by the ring-shaped design is 12.9%; more than a 2X improvement over the best reported results for optimized arrays of circular subapertures[5]. A second benefit of the design is that since every aspheric segment resides at the same radius, each has exactly the same prescription. This yields significant manufacturing savings due to common metrology equipment as well as enabling the option of replicated mirror technology. Lastly, because every segment is located immediately adjacent to a neighboring segment, simple sensors and reference features can be paired between bordering surfaces to seed the auto-alignment process with a much improved starting position.

The proposed architecture reduces the amount of polished mirror area and subsequently, the cost of the primary mirror array by the ratio of the fill factor; nearly an order of magnitude. Left is merely the engineering challenge of deploying a 30m wide structure from within an available launch fairing and maintaining the position of the collapsible optical structure to nanometer precision. Fortunately, two innovative Northrop Grumman technologies exist that, in combination, can be used to solve this deployment and alignment challenge. Northrop Grumman Astro Aerospace has extensive heritage and pre-existing investment in lightweight composite deployable structures for EHF (Extremely High Frequency) radio wavelength reflectors. The furlable AstroMesh product line achieves typical deployment accuracies of +/- 1mm at the 30m scale and is well suited for large circular truss structures. This accuracy serves as the starting point for a novel, iterative, automated alignment technique invented at AOX known as MIO (Modal Image Optimization). AOX has demonstrated phasing optics from this range with MIO technology for several years in numerous ground and airborne environments[6]. Descriptions of exactly how each of these technologies will meet their respective performance requirements are provided in later sections of this paper, but at the concept level, the proposed architecture appears to overcome all of the most pressing impediments to basing a 20 nano-radian resolution, visible imaging asset in space.

Another very interesting advantage of the proposed highly obscured telescope design is that it provides room for a second telescope (very wide FOV Schmidt-Baker ATMA) to actually be co-boresighted through the ID of the annular secondary mirror. This enables two modes of operation: very wide field scanning for search and detection, possibly even with a multi-spectral camera, and extremely high resolution at visible wavelengths.

3. DESIGN OF THE SEGMENTED PRIMARY MIRROR

Many methods are currently available to provide suitable materials and polished surfaces for the mirror segments, individually[7, 8]. However, because the number of mirrors is so large, achieving the goal of operating the observatory within an appropriate timeframe for space missions, roughly 10 years after award, eliminates several options from the trade space. Other considerations such as maximum launch payload mass, cost and technical risk also need to be matched against practical constraints. Cost information in Figure 3 was estimated from AOX's experience with these technologies, as they could be provided for a fully functional prototype testbed. Manufacturing costs for a true Class-A space program would be higher, including critical mission assurance factors outside the scope of this study, but it is expected that those would add proportionally to each of the options as a function of their base cost. Two polishing approaches and three candidate mirror materials were compared in a trade study, summarized below. Only proven, high-TRL manufacturing processes have been considered in the evaluation.

Longer geometries such as 3.1m x 1.0m glass segments were considered for the benefit of reducing the total quantity needed to fill the annular aperture, but these came with several disadvantages that eventually outweighed any savings. Significantly higher aerial density, higher cost substrate manufacturing and higher risk polishing were among the drawbacks. The first conclusion drawn from the above trade study is the mass of the Frit-bonded glass approach appears to be prohibitive for vehicles available in the proposed launch timeframe. Additionally, the cost, and more significantly, the schedule of producing 70 Low Temperature Fusion (LTF) mirrors do not appear to meet near-term funding constraints. For these reasons, silicon carbide is chosen over glass. It should also be noted that the trapezoidal shape of the mirror segments brings additional cost and complexity to the polished options. Alternatively, the replication process is ideally suited for this geometry. Additionally, because each of the primary mirror segments has an identical aspheric prescription, significant savings can be realized by requiring only a single mandrel prescription for high volume production. For this reason, replication was chosen over traditional polishing.

Parameter	Frit-bonded glass segments	LT-Fusion glass segments	Polished SiC segments	Replicated SiC segments
Number of mirror segments	70	70	70	70
Mirror segment size	1.34 m x 1.0 m	1.34 m x 1.0 m	1.34 m x 1.0 m	1.34 m x 1.0 m
Substrate cost (per mirror, high qty)	$0.4M	$3M	$0.3M	$0.3M
Polishing cost (per mirror, high qty)	$2M	$2M	$2.1M	$0.2M
Mount costs (per mirror, high qty)	$0.2M	$0.2M	$0.2M	$0.2M
Mirror fabrication NRE	$2M	$2M	$2M	$10M
Total cost of mirror segments	**$184M**	**$366M**	**$184M**	**$59M**
Substrate schedule (per mirror, high qty)	8 weeks, 2 production lines	38 weeks, 2 production lines	8 weeks, 2 production lines	8 weeks, 2 production lines
Polishing schedule (per mirror, high qty)	50 weeks, 6 production lines*	50 weeks, 3 production lines	50 weeks, 6 production lines*	4 weeks, 1 production line
Delivery schedule (first - last)	**11 years**	**26 years**	**11 years**	**5.4 years**
Substrate aerial density	100 kg/m2	30 kg/m2	12 kg/m2	30 kg/m2
Substrate mass	**9400 kg**	**2820 kg**	**1128 kg**	**2820 kg**
Notes	* managing 12 polishers would reduce schedule by 2X		* managing 12 polishers would reduce schedule by 2X	

Figure 3. Mirror Material and Manufacturing Process Trade Study

Thermal performance is a highly debated topic between these materials and almost always requires detailed analysis and a well defined operating environment to determine a victor. The offsetting advantages of higher thermal diffusivity versus lower thermal expansion between the two elevate the comparison beyond simple calculations. In the authors' experience, conditions with more benign, slow moving transients tend to favor lower CTE glass, though not always significantly, and conditions where solar loads emerge from shaded areas quickly or dwell directly on the optical surface usually tend to favor cold-biased, heater-controlled Silicon Carbide. Although, again, true quantification of these trends requires detailed thermal analysis and is beyond the scope of this study, many conclusions can be drawn with reasonable confidence.

The requirement for continuous, uninterrupted imaging for example, including times of abrupt day/night transitions, represents a challenging operating dynamic due to the relatively fast nature solar / cryogenic boundary conditions change incidence. Also, for this geometry, any sun shield would have to be extremely large and almost certainly less cost efficient than the simple alternative of locally controlled heaters integrated in the mount supports behind each mirror segment. This implies that for both the glass and SiC options, regardless of how one material may perform relative to the other, some level of active temperature control will be required to maintain surface figure of the segments over the operational environment. Therefore both systems would need to bear the cost burden of local thermal control hardware, and any differences in cost between those control systems would likely be minimal. It's worth mentioning that since thermal control for each individual segment around the aperture would be self contained, populating the aperture with some SiC mirror segments and some glass segments is very possible. This may have the additional advantage of reducing total polishing schedule and risk by involving more suppliers as well as providing competition for the award of a greater number of segments to contractors demonstrating superior cost, schedule and technical performance.

The proposed mounting concept for the SiC segments follows AOX's standard design for high stiffness, thermally stable, lightweight mirrors. Nine inserts bonded into bores cast into the open back rib structure of the SiC distribute working loads over a large portion of the mirror area and interface to three lightweight, CTE-matched whiffletree structures. Six flexured struts span from here to the multi-segment strongback platform at 70 degree angles in a hexapod-like configuration. Three of the flexured struts would contain high reliability, flight-proven inch-worm actuators to provide the necessary degrees of freedom (tip, tilt & piston) for aligning the segment with the rest of the primary surface. The inch-worm actuators have both coarse and fine mode control which provides the impressive combination of nanometer resolution during closed loop operation and several millimeters of range.

4. AUTOMATED ALIGNMENT OF THE SEGMENTS USING MIO

Modal Image Optimization (MIO) is a method of optimizing the surface of an active mirror by using nothing but the images produced at the focal plane. For a segmented aperture having at least three degrees of freedom per mirror, MIO adjusts the alignment of each segment individually and then phases them together. This section describes the algorithm, its constraints, and an approximation for the time required to perform the algorithm.

We begin with deriving requirements for the resolution of the image sensor and the initial alignment of the mirror segments. To fully resolve the images of a 30m diameter aperture, the focal plane array (FPA) pixels must have an

angular extent well inside the first dark ring of the Airy diffraction pattern. This is located at 1.22*λ/D, which for our design is approximately 22.4 nanoradians. For robustness, we chose 15 nanoradian pixels and used this as our baseline sensor for all imaging simulations reported later in this study. At this pixel spacing, providing the desired 200 microradian field of view (FOV) for high resolution images implies the detector plane must consist of an array of FPA's having ~178 megapixels in total. This is roughly twice the sensor resolution flown on NASA's Kepler mission, and 5X less than the FPA flown on ESA's Gaia mission.

Experience has shown that for MIO to have the highest reliability, the individual point spread functions (PSF) of each segment must fall on approximately the central half of the detector plane. A total FOV of 200 microradians therefore requires each segment to be optically aligned to ± 50 microradians before MIO can begin. From here, the position of the image on the FPA is observed, two additional tip, tilt positions are commanded and the coordinates that place the center of the scene on the center of the detector can be found by linear interpolation.

At this point the commands that produce high quality images on the optical axis are known for each individual segment but their phases are not coherent. Starting with the second segment, small steps in piston are driven, usually around 0.1 micron OPD, until the image contrast score is optimized. It is important to do these measurements broad band. A narrow band will produce a sharp image contrast peak every time a mirror steps through λ in OPD. A broad band image will have a distinct global maximum for the image contrast score. The three scores around the maximum are fit by a parabola to determine the optimum command, the segment is brought to this position, and the algorithm then moves on to the next segment. Once all the segments are phased, a second loop is usually repeated with a smaller step size to align the segments with higher accuracy.

The deployment mechanism described in section 6, is predicted to be able to place the segments to within +/- 1 mm based on measurements of previous systems at this scale. This tolerance is well within the 8mm range available from the commercial, high reliability inch-worm actuators in our baseline concept. We assume a secondary system such as edge sensors or a centralized laser tracker can handoff the segments' absolute position to within +/- 50 μm. The time required to command a change in piston to a segment, wait for it to settle, read out an image and calculate its score typically takes ~2.2 seconds per step. The tip and tilt modes only require 4 scores per segment, which can be completed for all 70 segments in less than 0.2 hrs. The first phasing pass requires: 1000 steps x 2.2 sec / step x 70 segments = 43 hrs. The final phasing pass using steps as small as .005 μm can be completed in less than an hour, including tip and tilt optimization.

5. DESIGN OF THE TELESCOPE

The telescope is comprised of a 30m diameter, on-axis, f/.27 Mersenne beam compressor, in front of a 1.5m Baker-Schmidt TMA. The front end telescope has a 30m diameter, annular primary mirror and a 1.5m convex, annular secondary mirror. Both optics have an obscuration ratio (D_i/D_o) of 93.3%. The surface was selected to be parabolic with a focal length of 10m. This extraordinarily fast curvature was chosen so that the entire telescope, once deployed, fits within an envelope of 30mØ x 10m. The secondary was chosen to be a 1.5m diameter parabola with a 0.5m focal length in an afocal Mersenne configuration with the primary. The Mersenne beam reducer produces little or no aberrations and compresses the light to a more manageable dimension of about 1.5m. Ray tracing analysis was performed to verify that the design can produce diffraction limited images over the intended 200μrad field of view. In fact, the design was shown to be well corrected, accumulating only 3nm rms WFE at off-axis positions of +/- 100μrad. The collimated beam feeds into a three mirror anastigmat (TMA). The first TMA mirror is a 1.5m diameter parabola with a 8m focal length, the second mirror is a 1m diameter conic with a focal length of 3m, and the third mirror is a 1m sphere with a focal length of 4.8m. The entire optical path of the TMA is 9.6m from the sphere to the focal plane. This is one example of a TMA that can meet our requirements, however, a F/11.1 TMA was actually simulated in the imaging results section. We note that an allowance for the slightly increased volume of this modification is necessary for future use. The effective focal length of the Mersenne and the simulated TMA together is about 333m.

The high resolution mode field of view was chosen to be limited by current detector design. Assuming a 13,333 x 13,333 detector array with a pixel size of 5 microns, the entire field of view is p*N/f = 5.0e-6m * 13,333 / 333m = 200 microradians. The TMA design was verified to produce diffraction limited images for the wide FOV mode as well with about 600 microns of field curvature from center to edge of the 5cm field of view. Other TMA designs exist that can eliminate the field curvature and may be pursued for future concepts. The graphic below outlines the configuration of the optical surfaces. The entire structure is about 30m wide and 10m tall.

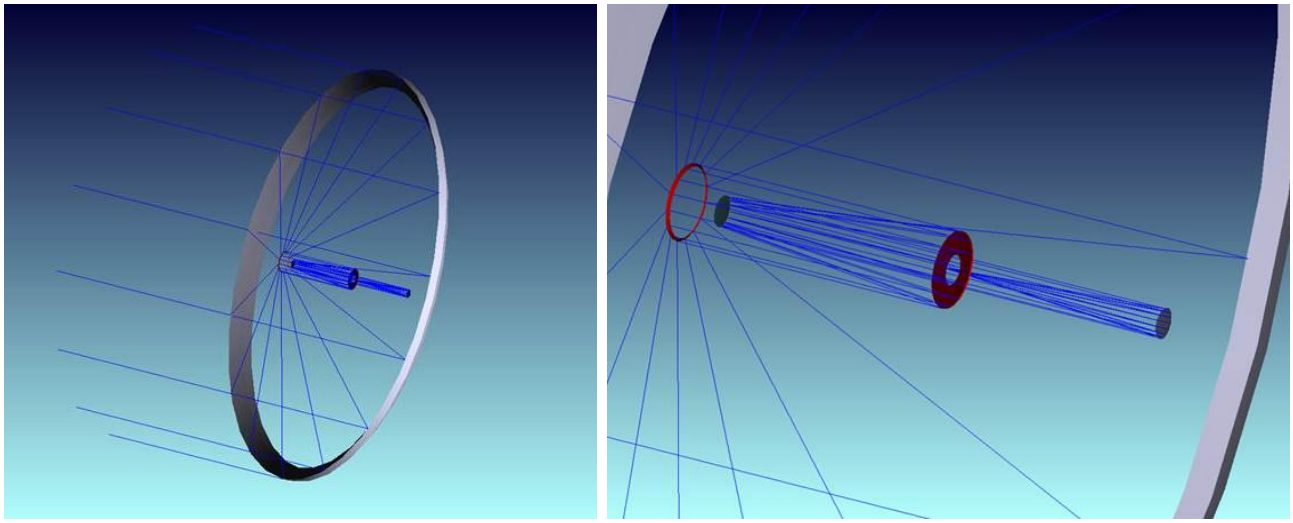

Figure 4. Ray trace view of the deployed 30m annular primary mirror (left), and zoomed-in view of the annular secondary mirror / ATMA assembly (right), highlighted in red.

The Baker-Schmidt TMA was derived from the Schmidt camera by James G. Baker in 1940, which is a very compact design with a spherical imager as the tertiary. The only drawback associated with this type of telescope is the lack of accessible cold shield, which is critical to sensors operating at the infrared spectral band. One way to correct this deficiency is to replace the spherical imager with an ATMA as shown in Figure 5. The size of the ATMA assembly is approximately 1.5mØ x 2.32m.

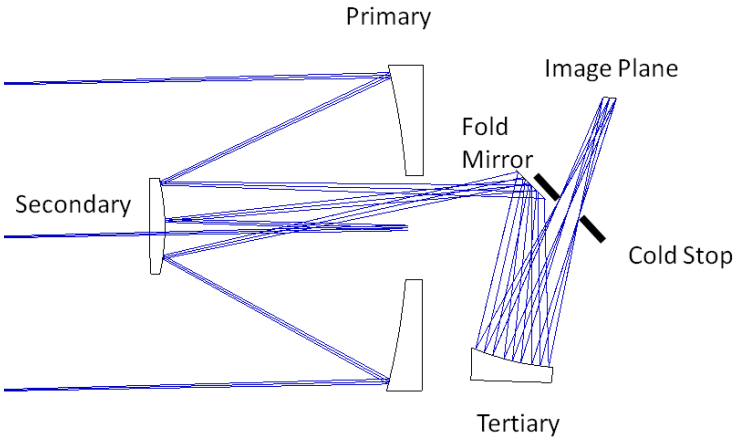

Figure 5. Ray trace view of only the beam path inside the ATMA.

The ATMA can bypass the front-end Mersenne telescope to have a 1.35 m, 4000 microradian field of view. This mode is ideal for search and detection. Activating the wide field of view mode is easily accomplished by aperturing down the cold shield by 10% to block the incoming light from the front-end telescope.

6. LAUNCH AND DEPLOYMENT OF THE TELESCOPE

The primary mirror segments need to be deployed to a highly accurate position by a thermally stable and reasonably stiff support structure to accommodate on orbit perturbations and maneuvering. A design that can meet all of these requirements is the patented, flight proven, AstroMesh^{TM} Perimeter Truss Reflector from Northrop Grumman Astro Aerospace. This truss was originally developed to deploy parabolic mesh reflector antennas. Currently, 9 of these are on

orbit on various spacecraft including Thuraya, MBSAT, Inmarsat, and Alphasat. These antennas stow in a compact cylindrical shape and deploy into a large circular truss as shown. The system is capable of deploying large panels as demonstrated by the Technology Development for Exoplanet Missions (TDEM) program which used this technology to deploy its occulter. The deployment of this was featured on the Science Channel's "Alien Planet Earths". Many aspects of the TDEM's occulter deployment are identical to how the proposed 30m ring telescope structure will deploy.

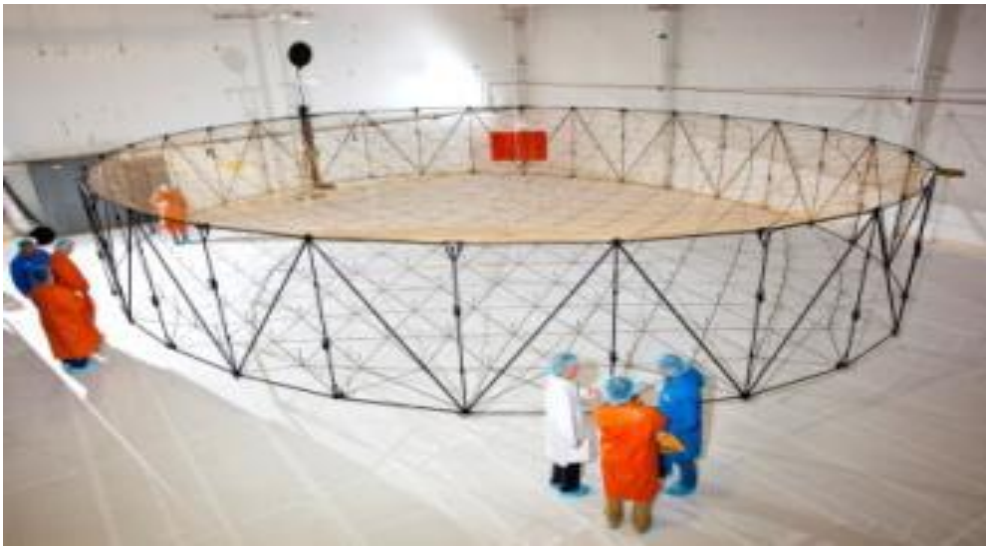

Figure 6. Verification testing of the Alphasat reflector at Northop Grumman Astro Aerospace's cleanroom facility in Carpinteria, CA.

The mirror segments attach to the truss vertically around the outside perimeter as shown in Figure 6. The truss is stowed around the outside of a central tower that provides support for the perimeter truss structure and the secondary mirror/TMA assembly for launch. After launch, the reflector is released from the central tower and pulled open by a cable drive system that also preloads the tension spokes. The mirror platforms attach to the truss through precision pivot joints which guide the rotation from their stowed position to a flat ring structure as the truss deploys. The truss is attached to the central tower with highly mass-efficient tension spokes, which stow in a relaxed configuration and become taut when fully deployed.

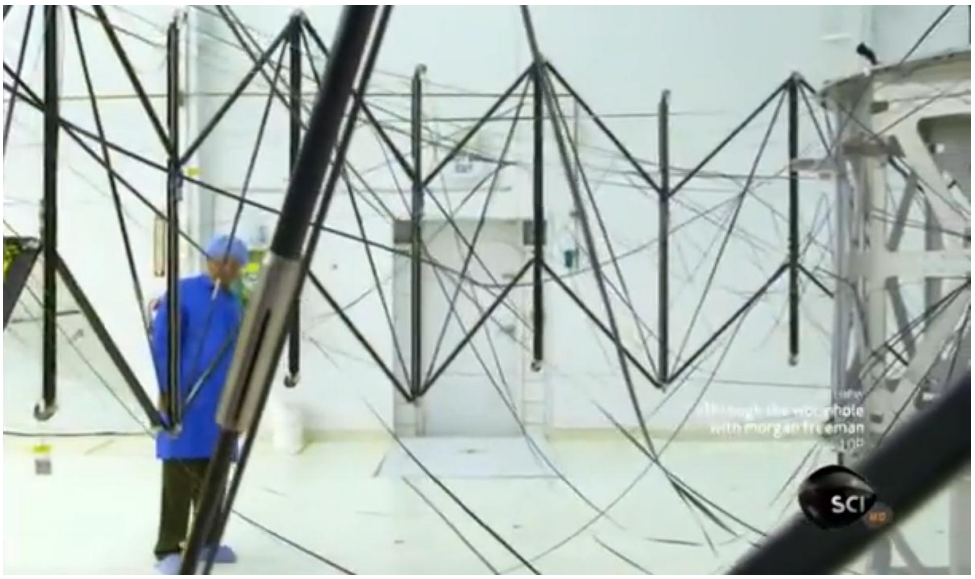

Figure 7. Verification testing of the TDEM occulter, as aired on the Science Network in 2007.

The truss now becomes a locked, preloloaded tension-compression structure with characteristically high specific stiffness. Preliminary calculations show that the deployed frequency of the system can be tailored between 1-4 Hz by changing the dimensions of the spokes, including a mass margin of 25%. This is a typical frequency range for successful on-orbit frequency performance among Astro Aerospace's previous space programs. The structure will also have significant damping. Combined with the predicted first frequency, the mechanical behavior of the system should be adequate for on-orbit performance, where it is convenient for vibrations from maneuvers between missions to settle out in less than about 30 seconds.

The 70 mirror segments are mounted in groups of 5 on 14 rigid platforms. These platforms attach to the truss at every other corner node giving the truss 28 bays around. The platforms provide support for launch of the mirrors and rigidly attach to the central tower for launch via release devices. After deployment, the platforms serve as a reaction structure for alignment of the mirrors. Deployment will be accomplished in the following sequence once on orbit:

1. Release launch locks for the telescopic mast and any attachments of the mirror segments and their supporting truss to the central mast support tube.
2. Turn on a motor which uses a cable to deploy the central ring truss. As the truss deploys the mirror segments rotate into a horizontal position. The truss locks itself into the deployed position.
3. Deploy the secondary mirror and TMA on the telescopic mast until it locks in place
4. Once deployed and locked into their initial alignment positions, the mirror segments can then be phased with the final auto-alignment process described previously.

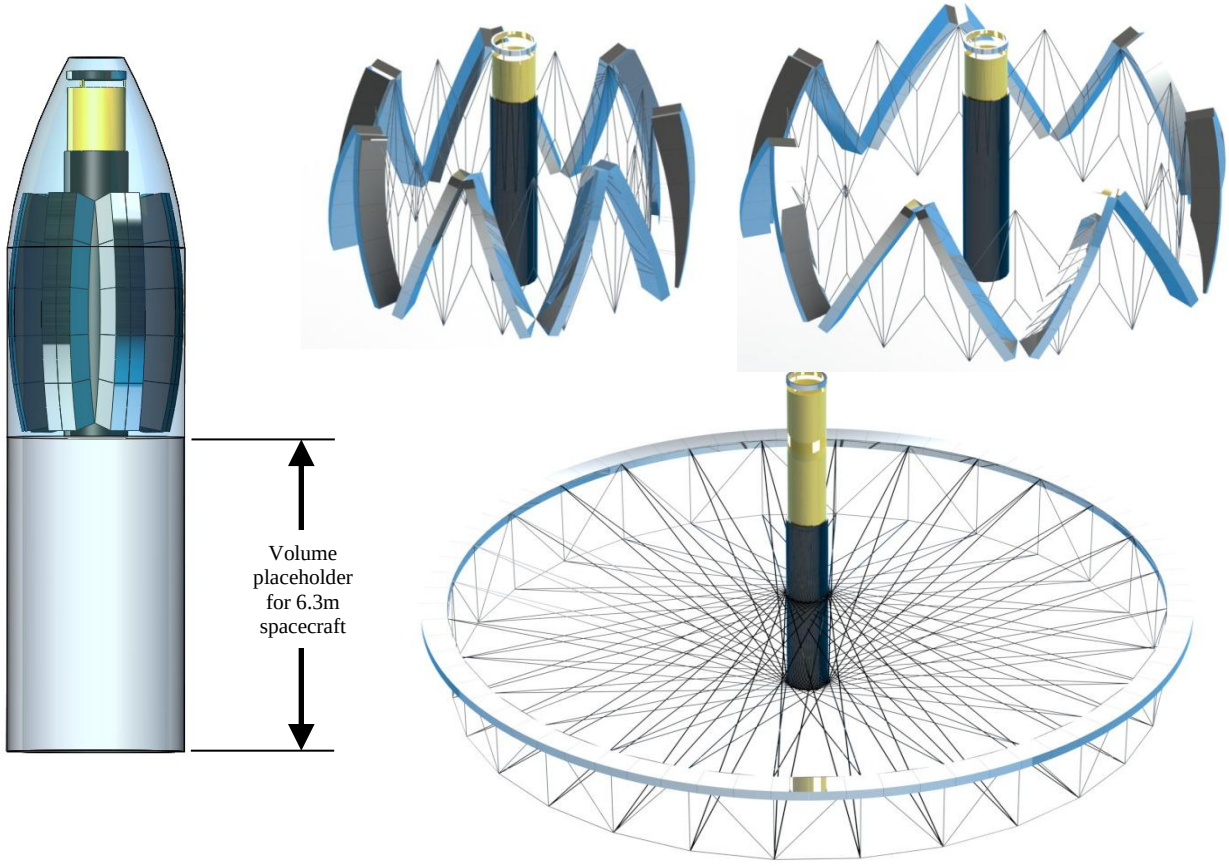

Figure 8. Conceptual rendering of the proposed 30m telescope as stowed in an Atlas-V launch fairing, at two intermediate steps of its deployment (shown with the spokes removed), and in its fully deployed configuration (including the central tension spokes).

The absolute position of the nodes of the truss will vary an estimated +/- 3mm, however, most of this can be calibrated out during ground testing. The repeatability from deployment to deployment will be better than +/- 1mm, well within the actuation range of the auto-alignment actuators. As for stability, preload of the truss inwards by the tensioned spokes can be adjusted to prevent micro slipping, and if deemed necessary, locks can be provided at all the clevis joints in the structure to create a virtually monolithic body.

The central tower is a stiff and stable graphite epoxy telescopic mast that deploys the secondary mirror approximately 10m away from the primary surface plane. Figure 8 illustrates the payload relative to an Atlas V 500 series long launch fairing[1]. The curvature of the stowed segments allows them to be partially tucked into the tapered portion of the fairing leaving a 4.6mØ x 6.3m volume for the spacecraft in the straight section of the fairing. The other pictures show the structure in various steps of deployment. The tension spokes are difficult to see despite being modeled slightly oversize to enhance their visibility.

The rendering of the perimeter truss is shown with relatively thin struts, however, the provided mass estimates used properly sized struts. All the masses are reported with 25% margin so it is expected that the payload mass is conservative. Also shown in Figure 9 is a comparison of the weight of the system relative to the launch capacity from which a mass allocation for the spacecraft can be derived.

Configuration	12" Thick Array Panels	16" Thick Array Panels
Mirror Segment Type	Active	Passive
Mass margin	25%	25%
Total mirror mass with margin(kg)	1939	3635
Total mast mass with margin (kg)	351	387
Total mass of truss with margin (kg)	345	275
TMA Mass (kg)	170	170
Total mass of truss, mast, mirrors, TMA with margin(kg)	2804	4468
Maximum payload mass to GTO Atlas V 500 Series(kg)	8900	8900
Maximum payload mass for spacecraft (kg)	6096	4432
Stowed natural frequency, First Mode (Hz)	10.2	11.5
Deployed first mode natural frequency using heritage material(Hz)	1.5	1.1
Deployed first mode natural frequency using tailored material(Hz)	5.7	4.4
Fairing inside diameter(m)	4.60	4.60
OD of system stowed for launch (m)(Maximum is 4.57m)	3.97	4.42
Maximum length in payload fairing for complete system (m)	16.5	16.5
Length available for spacecraft in fairing(m)	6.34	6.34

Figure 9. Design requirements table for the telescope's deployment mechanism

Detailed predictions for the natural frequency of the stowed system requires further analysis, but estimates using the telescopic mast outer tube as a mechanical ground and distributing the mass of the mirrors and truss over its length, yield a first mode natural of 10-12 Hz, as shown. Stiffer support is possible with additional strut elements, however, a first frequency above 10Hz is usually acceptable for precision instruments of this size and using the base section of the telescopic mast as the launch support simplifies the system. We note that other deployable optical structures, such as the hinges designed for JWST, may offer higher performance in certain design areas and future efforts should consider this option in the trade space relative to the requirements of the specific mission.

7. MANUFACTURING PLAN

Northrop Grumman AOX's replicated mirror technology combines years of development of two complementary innovations into one standardized process. Magnetron sputtered nanolaminate foils having the ability to produce optical quality replicas of polished surfaces were developed by Dr. Troy Barbee at the Lawrence Livermore National Laboratory and subsequently transferred to Northrop Grumman's National Replicated Optics Facility (53 Jackson, Devens, MA) in

2010 by the U.S. Government. The process of replicating an optical surface begins with depositing many layers of zirconium copper and reflective coating material onto a polished, usually convex mandrel. Once this is complete, a mirror substrate roughly generated with the opposite curvature is carefully bonded on top then mechanically released along the weak atomic interface between the mandrel and the first deposited layer of the nanolaminate. The final step is laser trimming excess foil material around the perimeter and sealing the exposed edge. The substrate then possesses the exact same surface quality, less any manufacturing errors, that was polished into the glass mandrel usually after significant time and expense. Fortunately, the AOX optical replication process, utilizing a single production line, can complete in as little as 4 weeks from start to finish with high volume tooling in place.

Fabricating a sufficient quantity of silicon carbide substrates to feed the proposed production line can be accomplished with relatively simple upgrades. The manufacturing process is currently optimized for production of 1.35m substrates at 8 week centers, however the process is mainly labor driven, so it can be scaled relatively easily to double the output. Moderate equipment upgrades, estimated around $3.5M, would be added to facilitate the increased capacity, but no building modifications or additional floor space would be required.

It's worth noting that primary mirror segments of this size and curvature would not be possible to manufacture at any other SiC provider. First, the uniformity and near-zero shrinkage property of the Xinetics Ceraform SiC recipe is a must. Years of experimentation and practice have led to the achievement of less than a 0.1% difference between the mold designed shape and final fired surface. This is unparalleled anywhere else in the industry, and absolutely essential for the manufacture of precision optics. In addition, the accumulated experience and extensive investment in high value, precision automated grinding machinery enables Xinetics to rapidly generate any optical surface imaginable, from axisymmetric to steep slope off-axis geometries to within 10-15μm of prescription.

The creation of Xinetics Ceraform SiC is a finely tuned, highly standardized manufacturing process that remains one of the few remaining critical technology materials produced in the United States. Its rapid production capability has benefited greatly from the scheduling algorithms and part sequencing developed during productions over the past 10 years. The Ceraform process begins with the formulation of the SiC slurry. The blending procedures used to form the SiC slurry from the raw powders, and the size of the batch made during the blending have been adjusted to take advantage of the information gathered on earlier programs. The fugitive core mold is then designed and machined into a separate material enclosed within a graphite case. Molds are generated to virtually any shape using a CNC machine. The slip of SiC powder suspended in water is poured into the mold in a carefully instrumented casting process. The part is then frozen and the mold material is leached out. The part is then vacuum-dried to extract the moisture from the slip. Finally, the case is placed in a precision-controlled vacuum furnace, and the part is fired at high temperature.

The fugitive core process described here is well suited to high production, replicated manufacture of near net shape optics. Molds are easily generated using computer-controlled milling machines. The designed part experiences less than a 0.1% linear change due to shrinkage. Careful selection of the SiC powder size permits complete flow into the mold, and yields a final part with a microstructure that can be direct polished, Si-clad, or transfer bonded to a replicated nanolaminate surface. In all cases, the final part has outstanding strength, durability and toughness.

After final firing, the part undergoes generation of the facesheet, to match the optical prescription for the part. This process has benefited from years of experience and lessons learned on previous SiC programs to steadily increase the accuracy and efficiency with which the prescribed surface can be iterated to. The generation process begins with blocking, or physical mounting onto a conformal backing structure that directly supports the back of the facesheet so that grinding pressures do not cause print-through of the rib structure onto the front surface. Surface generation utilizes AOX's Campbell grinder machine, a computer-controlled 3-axis grinder which is capable of generating surfaces on mirrors up to 2.5m in size. Surface generation is carried out in multiple stages, with the mirror being released and then reblocked between stages for strain relief and minimized iteration. Experience indicates that this can be completed to a precision of 10-15μm, depending on slope characteristics. More accurate machines, better machining practices, higher quality mold materials, and more powerful software, allow corrections for these distortions to be built into the process so that first iteration accuracy is optimized and major efficiency gains are realized. These corrections, coupled with improvements in casting and firing uniformity, have resulted in productions with tighter tolerance bands as well as higher part-to-part ROC uniformity relative to prior programs.

8. OPTICAL PERFORMANCE PREDICTIONS

Simulations were performed to predict how well the proposed design can resolve ISR-type images in realistic, on-orbit conditions. A description of the mathematical model is provided. The annular pupil function or pupil mask is first represented as a two dimensional matrix. The pupil point spread function (PSF) is then calculated by the square of the amplitude of the Fast Fourier Transform (FFT) of the pupil function. The input image is convolved with the PSF to generate the intensity distribution that a detector at the telescope image plane would see[9].

$$\text{Image detected from filled aperture} = \mathbf{FT}^{-1}\left(\mathbf{FT}(\text{scene})/\mathbf{FT}(\text{PSF}_{\text{filled}}) \right) \quad \text{Eq. 1}$$

$$\text{Image detected from annular aperture} = \mathbf{FT}^{-1}\left(\mathbf{FT}(\text{scene})/\mathbf{FT}(\text{PSF}_{\text{annular}}) \right) \quad \text{Eq. 2}$$

In practice, the pupil function is calculated using 0.1m pixels on a background of 4000x4000 pixels to avoid artificial numerical effects. The 30m diameter pupil used in the simulations produces a PSF with about 1.47 pixels peak to first null. Assuming a visible wavelength of 0.55 microns, the angular pixel size in the simulated PSF is approximately $(1/1.47)*(1.22*\lambda/d) = 15.2$ nanoradians.

The captured image from an annular telescope will appear degraded relative to the same scene taken with a filled aperture due to the inherent suppressions in the annular pupil's PSF. Fortunately, the information is still present in the annular case, it just needs post processing to be restored. The images below are an example of what a scene would look like through a filled 30m aperture and a 30m annular aperture with a 28m inner diameter.

Figure 10. Raw image data from a fully filled pupil (left), and a thin, annular pupil (right), prior to post-processing.

Notice in Equations 1-2, by substituting the annular telescope's formulation of the idealized scene into the equation for the filled image, we can derive an expression for the filled aperture's image in terms of the annular aperture's information. This operation can be used to effectively boost the contrast of spatial frequency content suppressed in the annular image. This is a standard post-processing technique for restoring images with known aberration characteristics.

$$\text{Restored Image} = \mathbf{FT}^{-1}\left(\mathbf{FT}(\text{Image}_{\text{annular}}) \times \mathbf{FT}(\text{PSF}_{\text{filled}})/\mathbf{FT}(\text{PSF}_{\text{annular}}) \right) \quad \text{Eq. 3}$$

The Fourier transform of a system's PSF is referred to as its optical transfer function (OTF). Care must be taken to zero the amplitude of this complex matrix for spatial frequencies beyond the limit imposed by the diameter of the pupil. Of course if any spatial frequencies of a pupil's OTF are completely absent, there is no information to boost and a division by zero error will occur. Likewise, if a system's OTF suppresses content so much that amplitudes are very close to zero, then the restoration process in Equation 3 will amplify the image noise in that domain beyond interpretable levels. It is

useful to plot the modulus of the complex OTF (known as the MTF) to visualize how much amplification needs to occur to restore an image to that of a filled pupil. This is shown in Figure 11 below, for 3 pupils of increasing obscuration.

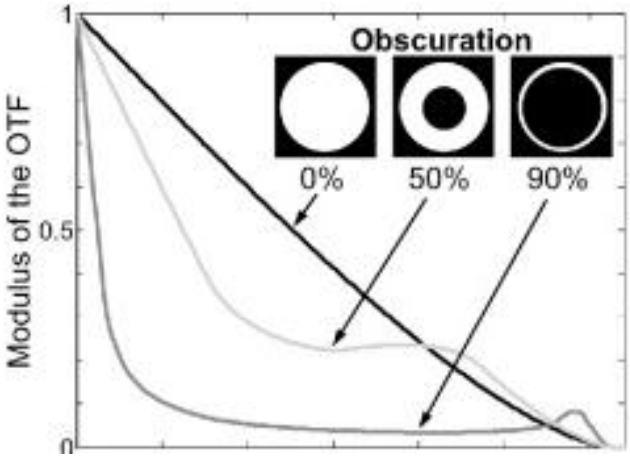

Figure 11. Plots of MTF vs. spatial frequency for three pupils of increasing obscuration. Graphic courtesy of Tremblay, et al.[10]

The lower limit of 3% MTF-peak used to arrive at the proposed design does not require the input image to have unobtainably high signal to noise ratios (SNR). This was confirmed by simulating several scenes and restoring the detected image using Equation 3 from a simulated annular telescope of our proposed dimensions, and injected with varying degrees of noise in the bright areas of the image. Shot noise is kept low by capturing at least 250,000 photons per image with less than 0.1 second exposures. The telescope's large light collecting area (>90m^2) and reasonably bright scene (>>0.2W/m^2/steradian) make this easily achievable. The results are shown below in Figure 12. Additionally, to generate sample images which represent the performance of a real system, full allocations for wavefront error (WFE) and SNR contributions were chosen be included in the simulation. As such, top level error budgets were derived in Figure 12, below.

Error Source	**WFE (nm rms)**
Surface Figure	38
Alignment	10
Thermal Loading	38
Total (RSS)	**54.7**

Error Source	**SNR**
Optic Surface Roughness	300 :1
Stray Light	200 :1
Shot Noise & Electronics	400 :1
Total (RSS)	**154 :1**

Case #	Aperture	RMS WFE	SNR	Image performance
1	30m OD, filled	0	1000	NIIRS 6
2	30m OD, 28m ID	0	1000	NIIRS 6
3	30m OD, 28m ID	.055 um	1000	NIIRS 6
4	30m OD, 28m ID	.055 um	300	NIIRS 6
5	30m OD, 28m ID	.055 um	150	NIIRS 6
6	30m OD, 28m ID	.055 um	100	NIIRS 5

Figure 12. Allocated error budgets for system level wavefront error and detected image noise (top). Results of image simulation cases considered, with interpretabilities as judged using the NIIRS criteria (bottom).

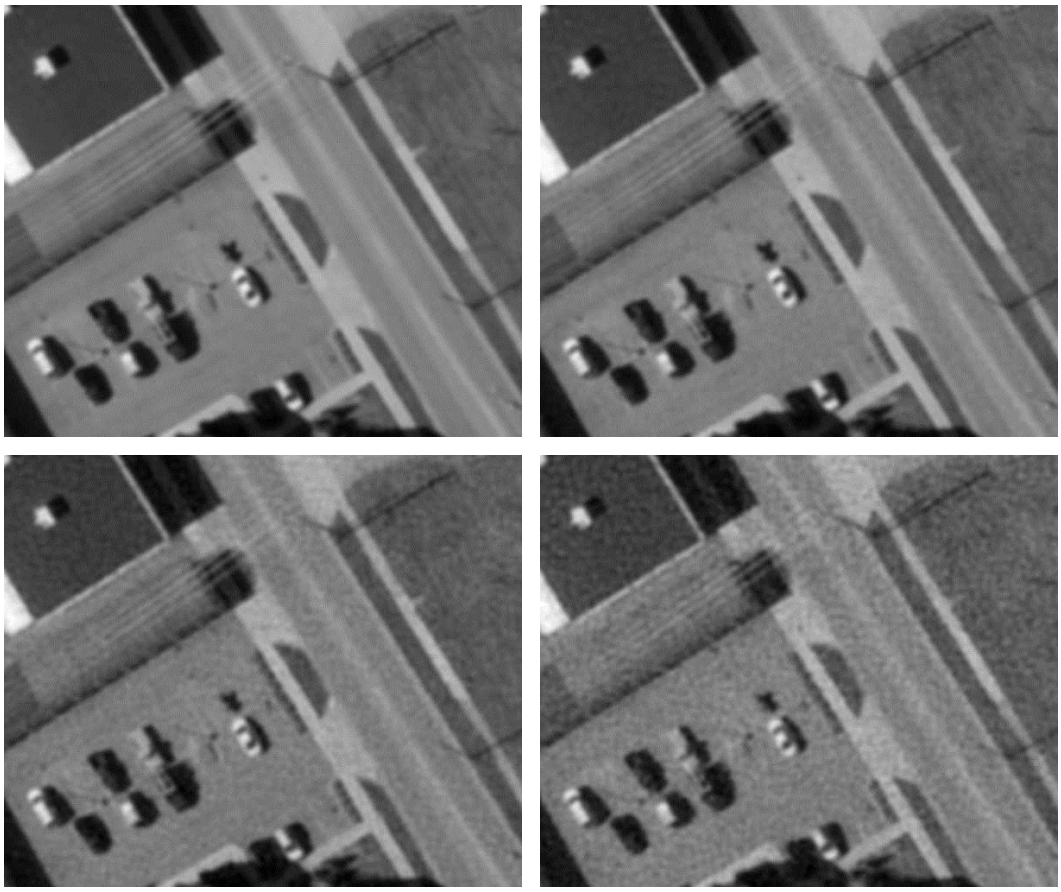

Figure 13. Image data from the simulated, annular, 30m telescope, for four scenarios of increasing signal-to-noise ratio, after image post-processing: (1): SNR = 1000:1, (2) SNR = 300:1, (3) SNR = 150:1, (4) SNR = 100:1.

The interpretation requirements for NIIRS levels are somewhat subjective and depend on the experience of the observer, however some guidelines are published. A common criterion for NIIRS-6 is the ability to differentiate between similar size vehicles of different type. We felt this could be done in case 5, but not reliably in case 6. In summary, a straightforward image post processing technique can be used to reconstruct scenes from images taken with a 30m annular aperture to produce essentially equivalent utility as a filled aperture for image interpretation on the NIIRS scale. No spatial frequencies are lost, and modest image signal to noise ratios are required for usable reconstructed images. The architecture can also be easily adapted for specific environments with higher intrinsic noise levels by increasing the width of the pupil ring to raise the MTF floor to the desired amplification ratio, at the cost of increased fill-factor.

9. CONCLUSIONS

It is shown that the proposed 30m segmented annular telescope design achieves essentially equivalent image interpretability and scene resolution, after post-processing, as idealized, monolithic 30m designs. Significant cost reductions are also demonstrated due to several factors. Mirror fabrication and polishing costs are reduced by eliminating much of the total mirror area. Launch costs are further reduced by using superior lightweighted silicon carbide as the mirror material. Additional savings are also achieved by copying the polished optical prescription onto the 70 mirror segments with the use of AOX nanolaminate replicated mirror technology. Mass is well within launch limitations. Volume envelope is also within payload limitations after being compressed by more than a factor of 30X with the use of novel deployment structures from Northrop Grumman Astro Aerospace. Phased alignment can be

achieved with the use of commercially available rigid body actuators and an advanced iterative algorithm from AOX known as MIO. A very wide angle scanning mode (4,000 μrad FOV), co-boresighted with the high-power (.020 μrad resolution) telescope, is available due to the unoccupied beam space through the center of the annular secondary mirror. Northrop Grumman believes the proposed 30m space-based observatory presents a compelling case for next-generation imaging architectures and is excited about the prospect of providing such capability to our customers.

REFERENCES

[1] Atlas V – United Launch Alliance, "Atlas V Launch Services Users Guide March 2010" Revision 11, (United Launch Alliance LLC) P6-4, <http://www.ulalaunch.com/uploads/docs/AtlasVUsersGuide2010.pdf>

[2] Pike, J., "National Image Interpretability Rating Scales", <http://www.fas.org/irp/imint/niirs.htm>, 16 January, 1998.

[3] Miller, N., Dierking, M., and Duncan, B., "Optical sparse aperture imaging", Appl. Opt. 46, 5933–5943 (2007).

[4] Golay, M., "Point arrays having compact, nonredundant autocorrelations," J. Opt. Soc. Am. 61, 272–273 (1971).

[5] Flores, J., Paez, G., and Strojnik, M., "Design of a diluted aperture by use of the practical cutoff frequency", Appl. Opt. 38, 6010-6018 (1999).

[6] Wirth, A., Jankevics, A., and Landers, F., "Scene Based Wavefront Sensing for Figure Control of Airborne and Space Optics", OSA Adaptive Optics: Methods, Analysis and Applications, ISBN: 978-1-55752-878-0 (2009).

[7] Stahl, P., et al.,"Single variable parametric cost models for space telescopes" Opt. Eng. 49, SPIE 091-3286 (2010).

[8] Ealey, M., and Wellman, J., "Ultralightweight silicon carbide mirror design ," Proc. SPIE Vol. 2857, Advanced Materials for Optical and Precision Structures, p.73-77 (1996).

[9] Hecht, E., [Optics], Addison Wesley, San Francisco, CA. "Optical Applications", 530-544 (2002).

[10] Tremblay, E., Stack, R., Morrison, R., and Ford, J., "Ultra-thin cameras using annular folded optics," Appl. Opt. 46, 463-471 (2007).